Effect of *m*-Nitroaniline Doping on the Optical Humidity-Sensing Characteristics of Cobalt/Poly(vinyl alcohol) Nanocomposites

Parag Adhyapak,[1] Poonam Mahapure,[2] Rohini Aiyer,[2] Suresh Gosavi,[2] Uttamrao Mulik,[1] Dinesh Amalnerkar[1]

[1]*Centre for Materials for Electronics Technology, Panchwati, off Pashan, Pune 411008, India*
[2]*Department of Physics, University of Pune, Pune 411007, India*

Received 20 January 2011; accepted 8 May 2011
DOI 10.1002/app.34875
Published online 20 September 2011 in Wiley Online Library (wileyonlinelibrary.com).

ABSTRACT: Cobalt (Co) nanoparticles (with different loadings, 1 and 2 wt %, of Co) were synthesized *in situ* in a poly(vinyl alcohol) (PVA) matrix with and without *meta*-nitroaniline (*m*-NA) as a dopant (2.5 wt %). The obtained nanocomposite films were characterized with various physicochemical techniques, including ultraviolet–visible spectrophotometry, X-ray diffraction analysis, scanning electron microscopy, and Fourier transform infrared analysis. To study the effect of the humidity, the nanocomposite solutions were coated on planar glass substrates. The beam of an He–Ne laser was incident normal to the film surface and was subjected to variable relative humidities (RHs; 4–93%); the transmitted intensity was measured on a photovoltaic diode. Variations in the intensity of light caused by the changes in RH within the range 3–93% were recorded. We optimized the response by varying the film thickness by coating the solution layer by layer. We generated the RH (4–100%) by passing wet water vapors. The neat PVA film of similar thickness gave humidity sensing in the range 78–93% RH. The sensors with *m*-NA-doped Co/PVA gave better sensitivity (6.4 mV/% RH) than the undoped samples (1.78–2.45 mV/% RH), exhibiting a fast response of 3 s (2–93% RH) and a recovery of 10 s (93 to 2% RH). These samples also showed reversible behavior and long-term stability (for nearly a year) with a good sensitivity and a large dynamic range (2–95% RH). An attempt was made to explain the results on the basis of a bulk mechanism. © 2011 Wiley Periodicals, Inc. J Appl Polym Sci 123: 3565–3574, 2012

Key words: nanocomposites; nanoparticle; sensors

INTRODUCTION

In recent years, research on humidity-sensitive materials has attracted more attention because of their wide applications in industrial and agricultural production, process control, household electrical appliances, and so on. Depending on the need, humidity sensing is carried out by different methods, that is, resistive, capacitive, or optical. In the optical method, a change in the intensity of light with percentage relative humidity (RH) is measured.[1] The major factors affecting sensor response include the sensor size, film thickness, and number of hydroxyl sites.[2] A change in the number of hydroxyl sites quantitatively produces a change in the adsorbed water. Therefore, samples providing more sites are preferred. Presently, humidity sensors are based on polyelectrolytes and conjugated polymers because they offer more active sites. Polyelectrolytes are hydrophilic or even water soluble, whereas conjugated polymers (conducting or semiconducting polymers) are rather hydrophobic and are unable to absorb considerable amounts of water. Polyelectrolytes are polymers with electrolytic groups, which could be salts, acids, and bases. On the basis of functional groups, humidity-sensitive polyelectrolytes can be fundamentally divided into three major categories: quaternary ammonium salts,[3–5] sulfonate salts,[6,7] and phosphonium salts.[8,9] Ion-conducting polymeric systems have been used in humidity sensors on the basis of the variation of the electrical conductivity with water vapor. Polymer electrolytes containing a polymer cation/polymer anion with its counter ions and mixtures or complexes of inorganic salts with polymers are the major materials for humidity sensors, for example, poly(vinyl alcohol) (PVA).

Hydrophilic groups, such as $-SO_3^-$ and quaternary ammonium side group, exhibit a strong affinity to water molecules.[10] To fabricate humidity sensors based on polyelectrolytes, it is reasonable to use some methods to prevent deformation caused by dissolving[11] and to enhance the sensitivity by lowering the intrinsic conductivity.[12] It is well known that doped conjugated polymers and their derivatives are sensitive to

Correspondence to: P. Adhyapak (adhyapakp@yahoo.com or adhyapak@cmet.gov.in).

humidity with a fast response due to weak hygroscopicity.[13–16] To enhance the sensitivity, the polyelectrolytes need to be doped with ammonium salts.[4,17]

To take advantage of the tunable chemical and physical properties of polymers to increase the sensitivity and range of humidity sensing, a successful attempt was made to synthesize cobalt (Co)/PVA and *meta*-nitroaniline (*m*-NA)-doped Co/PVA metal–polymer nanocomposites in solution form. Here, the polymer acted as a matrix to disperse the metal particles. Thin films were deposited by spin coating on soda-glass substrates, and the samples were characterized optically in the RH range 3–100% RH for various thicknesses.

EXPERIMENTAL

The experiments were divided into five parts: material synthesis, characterization, sensor fabrication, humidity sensing, and measurement of the moisture content to determine the humidity-sensing behavior.

Preparation of the Co/PVA and *m*-NA-doped Co/PVA nanocomposites

To prepare the nanocomposites, 1 g of PVA was dissolved in 25 mL of water to form a viscous solution. To this solution, a 0.01*M* Co salt solution was added in the required quantity to make 1.0 wt % (ncp1) and 2.0 wt % (ncp2) Co loadings in the matrix (where ncp1 represents the 1.0 wt % Co-loaded sample and ncp2 represents the 2.0 wt % Co-loaded sample). The reaction mixture was stirred at room temperature to get a homogeneous mixture. A diluted hydrazine hydrate solution was prepared separately in water, and 20 μL of this solution was added by a microsyringe. The initial pale pink color of the solution changed to pale gray. To prepare *m*-NA-doped Co/PVA nanocomposites, the methanolic solution of *m*-NA (10 mL, 0.01*M*) was injected dropwise with a syringe, and the reaction mixture was stirred for 1 h; after doping with 2.5 wt % *m*-NA the samples were obtained and were named ncpn1 and ncpn2 (where ncpn1 and ncpn2 are the 1 and 2 wt %, respectively, Co-loaded samples doped with *m*-nA). The obtained nanocomposites were characterized with various characterization techniques.

Physicochemical characterization

The prepared nanocomposites were characterized with ultraviolet–visible (UV–vis) spectroscopy (Hitachi spectrophotometer model U-3210 (Japan)) for optical studies. X-ray diffraction (XRD) analysis was done on a Rigaku Mini Flex diffractometer with Cu Kα radiation (λ = 1.5405 Å, nickel filter). Fourier transform infrared (FTIR) spectroscopy (PerkinElmer Spectrum 2000) was used to determine the type of interactions in the polymer. Atomic force microscopy (AFM; NT-MDT Ntegra) and field emission scanning electron microscopy (FESEM; JEOL, JSM model 6700F) were used to study the surface morphology.

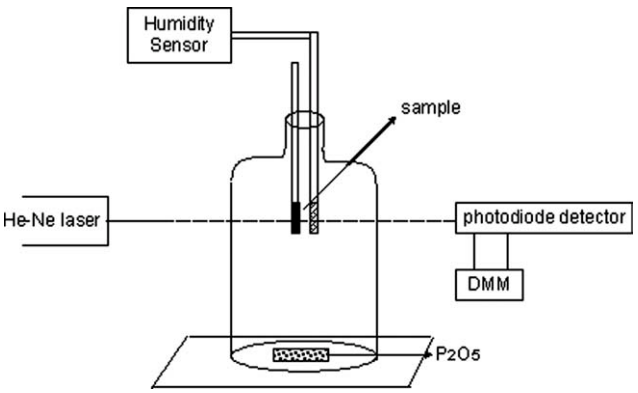

Figure 1 Experimental setup for studying the *m*-NA/Co/PVA-based humidity sensor with simple optical transmission.

To form films of *m*-NA-doped and undoped Co/PVA nanocomposites, solutions were spin-coated (2 μL each) on a precleaned glass substrate with dimensions of 1 × 1 cm^2 (for 10 s at 2000 rpm), here with one layer corresponding to 2 μL. The next layer was coated after the previous layer was dried. The prepared films were studied for their sensitivity toward humidity.

Humidity-sensing measurements

The experimental setup for the characterization of the humidity response is given in Figure 1. It consisted of a glass chamber, a He–Ne laser (0.95 mW), a sensing sample (*m*-NA-doped and undoped Co/PVA films) and a detector (photovoltaic detector). Laser, the sensing sample and detector were optically aligned (parallel to each other). The sensing films were kept in the glass chamber, which was tightly closed to prevent air exchange and to maintain a constant humidity.

Hot water vapors were passed inside the glass chamber to create required humidity in the chamber, which was measured by a standard humidity meter (48 EU 05) inside the chamber for experimental purposes. P_2O_5 (Aldrich Chemicals) was used to dehumidify the glass chamber.

The transmitted light was incident on the film kept inside the chamber, and output light was directed on the photovoltaic detector (measured on $3\frac{1}{2}$ digital multimeter (DMM) least count 0.1 mV), which was kept outside the chamber. The output voltage as a function of RH was measured.

The single layer of the film could not cover the full RH range. To increase this range, the thicknesses of the samples were increased by the deposition of 2 μL of solution/layer, and the samples were spun. The sensitivity was measured as the change in

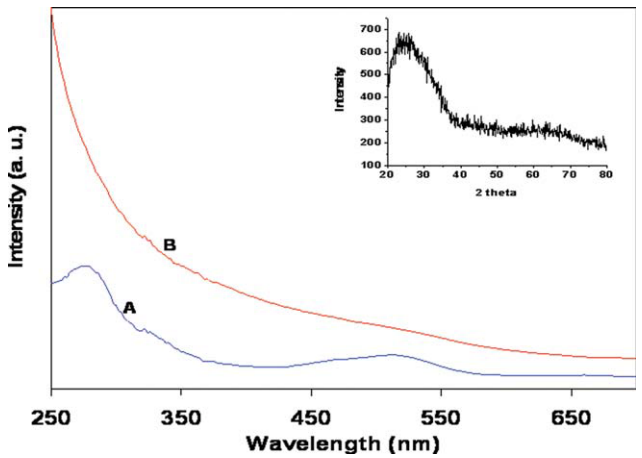

Figure 2 UV–vis absorption spectra of (A) the $CoCl_2$–PVA aqueous solution and (B) the formation of Co particles in the PVA matrix after reduction (ncp1; inset: XRD pattern of the resultant nanocomposite film). [Color figure can be viewed in the online issue, which is available at wileyonlinelibrary.com.]

transmitted output per unit change in percentage RH.[18,19] For convenience, the percentage normalized output was used to plot graphs for various thicknesses. The output was normalized with respect to voltage at lower humidity, that is

$$\text{Normalized output}(\%) = \frac{V_{lh} - V_{hh}}{V_{lh}} \times 100 \qquad (1)$$

Where V_{lh} is voltage representing resistance at lower humidity and V_{hh} is voltage representing resistance at higher humidity.

RESULTS AND DISCUSSION

Material characterization

The UV–vis spectra of cobalt chloride in PVA solution before and after reduction are exhibited in Figure 2. The solution before the addition of hydrazine hydrate showed two peaks at 280 and 512 nm (plot A). After the addition of hydrazine hydrate, the 280- and 512-nm peaks disappeared; this indicated

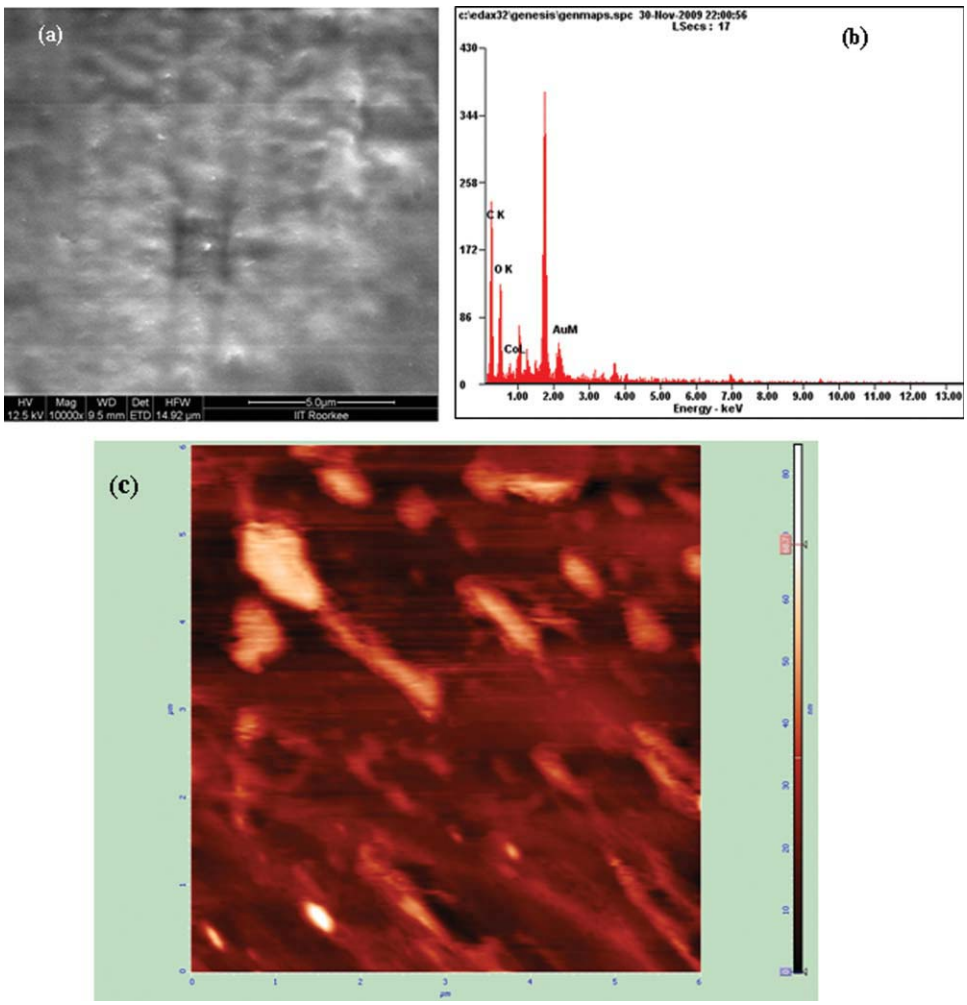

Figure 3 (a) FESEM, (b) EDAX, and (c) AFM images of ncp1. [Color figure can be viewed in the online issue, which is available at wileyonlinelibrary.com.]

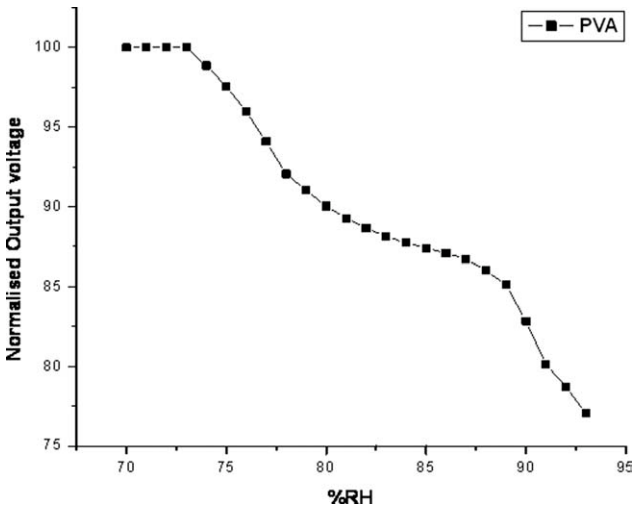

Figure 4 Humidity sensing for PVA.

complete reduction of Co^{2+} ions and the subsequent formation of Co particles. The color of the solution turned from pink to dark. The absorption from UV to the visible region increased (plot B).[20]

Figure 2 (inset) represents the XRD pattern of the representative Co/PVA nanocomposite film ncp1, which showed feeble evidence of Co formation because of a very small Co loading in the polymer matrix. The XRD pattern was amorphous in nature because of the polymer; however, very weak signals were observed at 2θ values of 41.69, 43.81, 49.34, 59.59, and 63.35°; this was attributed to the hexagonal phase of Co [Joint committee on powder diffraction standards (JCPDS) card No. 5-727]

The FESEM pictures in Figure 3 for ncp1 illustrate the surface morphological studies of the nanocomposite film and show the uniform distribution of Co. It is shown in Figure 3(a) that the particles were homogeneous. However, a few larger (~ 100–300 nm) and smaller (~ 25–50 nm) sized particles tended to agglomerate; this led to the formation of a rodlike structure. Such a type of self-assembly was also seen in the AFM image [Fig. 3(c)]. The energy-dispersive X-ray spectroscopy (EDAX) further confirmed the presence of Co in the sample. The peaks pertaining to Co were present in the EDAX spectrum [Fig. 3(b)].

Humidity measurements

Figure 4 displays the humidity-sensing results for pristine PVA. The normalized output voltage of PVA covered 27 units of output at the third layer, which was much higher than that of polyaniline, which covered almost 2 units of output, as mentioned by Fuke et al.[21] in an evaluation of Co–polyaniline nanocomposite thin films as humidity sensors.

All of the sensors of the undoped and doped samples roughly exhibited two to three regions of sensitivity with very low sensitivity at low humidity levels, increased sensitivity at medium humidity levels, and high sensitivity at high humidity levels. The first layer of undoped ncp1 and ncp2 covered a humidity-sensing range of 70–100 and 40–100% RH [Fig. 5(a)], respectively, with three regions of sensitivity, that is, 0.0240 corresponding to 3–54% RH, 0.2947 corresponding to 55–83% RH, and 1.3432 corresponding to 84–93% RH and 0.1847 corresponding to 4–34% RH, 0.4903 corresponding to 35–73% RH, and 0.7921 corresponding to 74–90% RH for ncp1 and ncp2, respectively. ncp2 had nearly an order of magnitude higher sensitivity than ncp1 at lower and higher humidity-sensing ranges. This was attributed to a higher number of Co nanoparticles, which offered a larger number of sites for interaction with water molecules because of higher concentration of Co.

The *m*-NA-doped samples covered a wider range of humidity with a single layer [Fig. 5(b)], that is,

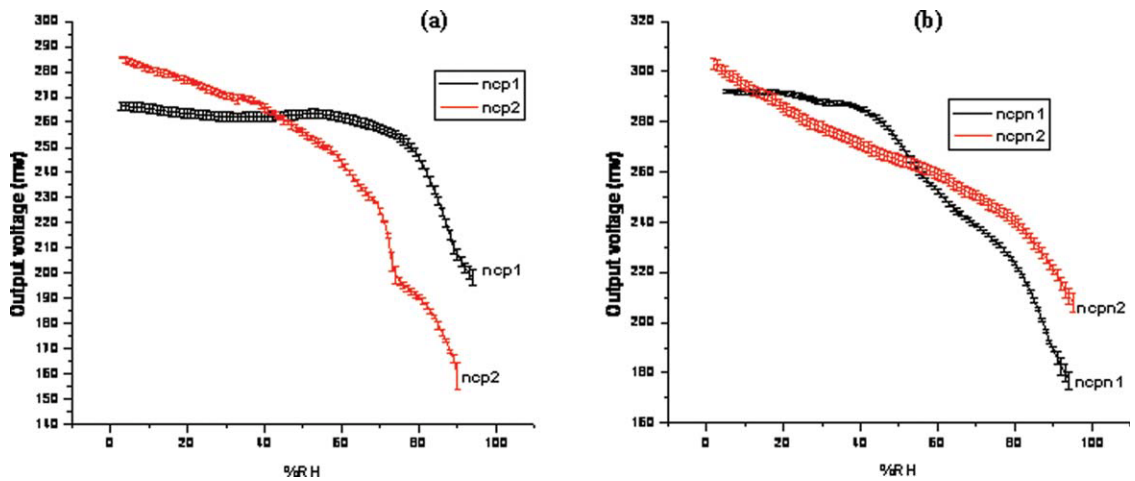

Figure 5 Variation of the output voltage with RH for the first layer of (a) ncp1 and ncp2 and (b) ncpn1 and ncpn2 with error bars. [Color figure can be viewed in the online issue, which is available at wileyonlinelibrary.com.]

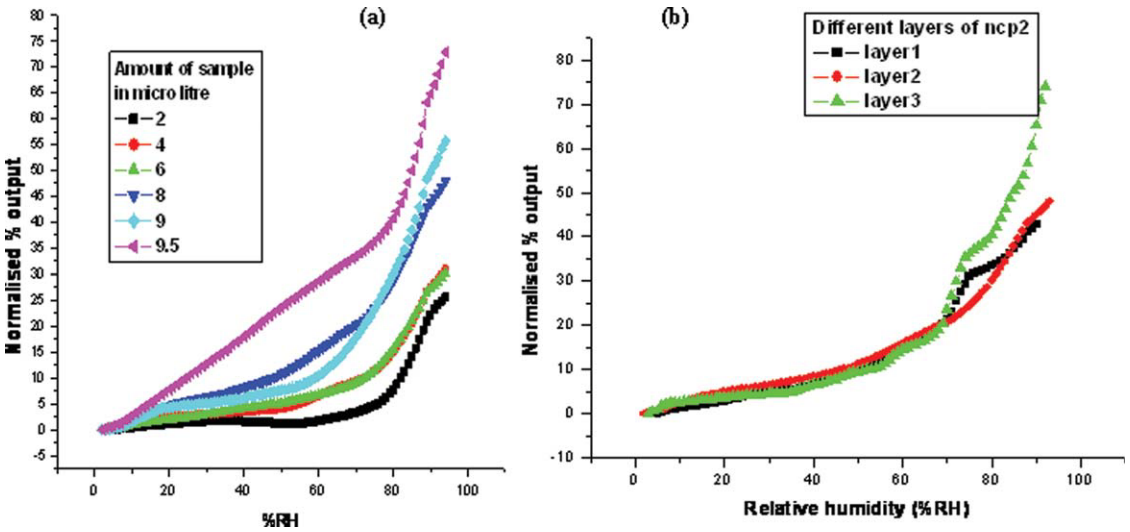

Figure 6 Variation of the percentage output voltage with RH for the number of layers for (a) ncp1 and (b) ncp2. [Color figure can be viewed in the online issue, which is available at wileyonlinelibrary.com.]

ncpn1 covered 33–94% RH, and ncpn2 covered 3–95% RH. ncpn1 and ncpn2 showed three and two regions, respectively, having sensitivities of 0.01292 (3–17%), 0.1038 (18–40%), and 0.64892 (41–93%) and 0.86913 and 2.46804, respectively. The overall sensitivity of ncpn2 was quite higher than ncpn1.

Effect of the thickness on humidity sensing

The thickness of the samples was varied to cover a better range of humidity sensing in the doped and undoped samples to determine the effect of the thickness on the sensitivity. Figure 6 displays the effect of the thickness for the undoped samples. The variations in optical output with the variations in percentage RH are plotted. The results are tabulated in Table I. ncp1 and ncp2 covered a maximum range of humidity, that is, 3–93% RH at layers of sample amounts of 9.5 μL (2 + 2 + 2 + 2 + 1.5 μL) and 6 μL, respectively. Above these thickness, the samples were totally opaque to the incoming radiation. For ncp1, the sensing mechanism was divided into three regions of different humidity ranges (Table I). The humidity-sensing range increased with increasing layers. The sensitivities of the second and third regions decreased with increasing number of layers (0.29 to 0.12 and 1.34 to 0.40, respectively, normalized output with respect to voltage at lower humidity) up to a sample amount formed by the placement of 2 + 2 + 2 + 2 + 1 μL of liquid, that is, 9 μL, of solution effectively (i.e., 4.5 layers). The first region (the low-humidity region) was an almost constant region, but the range of this region decreased continuously with increasing thickness and offered two regions with high sensitivity [0.51767 (3–79%) and 2.4590 (80–93%); Fig. 6(a), Table I].

TABLE I
Humidity Range and Sensitivity for Number of Layers for ncp1 and ncp2

Amount of sample (μL)	Sensitivity (mV/% RH)		
	Region I	Region II	Region III
ncp1			
2	0.0240 (3–54)	0.2947 (55–83)	1.3432 (84–93)
4	0.0756 (3–47)	0.2861 (47–78)	1.17087 (78–93)
6	0.1034 (3–27)	0.1575 (28–75)	1.06916 (76–93)
8	0.2645 (3–25)	0.1433 (14–50)	0.83711 (51–93)
9	0.2876 (3–16)	0.1298 (17–60)	0.4018 (61–93)
9.5	0.51767 (3–79)		2.4590 (80–93)
ncp2			
2	0.1847 (4–34)	0.4903 (35–73)	0.7921 (74–90)
4	0.2159 (3–35)	0.4035 (36–70)	1.31173 (71–93)
6	0.2267 (5–12)	0.2602 (13–64)	1.77202 (65–92)

For ncp2, the humidity-sensing range and sensitivity in all regions increased with increasing number of layers: 0.1847 corresponding to 4–34% RH to 0.2267 corresponding to 5–12% RH, 0.4903 corresponding to 35–73% RH to 0.2602 corresponding to 13–64% RH, and 0.7921 corresponding to 74–90% RH to 1.77202 corresponding to 65–92% RH [Fig. 6(b), Table I].

For the *m*-NA-doped samples ncpn1 and ncpn2, the sensitivity of both of the samples increased with the number of layers in all of the regions (Fig. 7, Table II). The ncpn2 sample was more sensitive than ncpn1, ncp1, and ncp2. In the low-humidity region, ncpn2 was more sensitive than ncpn1 and the undoped samples. After the third layer (6 μL), the sample was totally opaque to He–Ne beam light. The doped ncpn1 showed three sensing regions; here, the range of the first region increased with thickness and merged into two regions for layers of

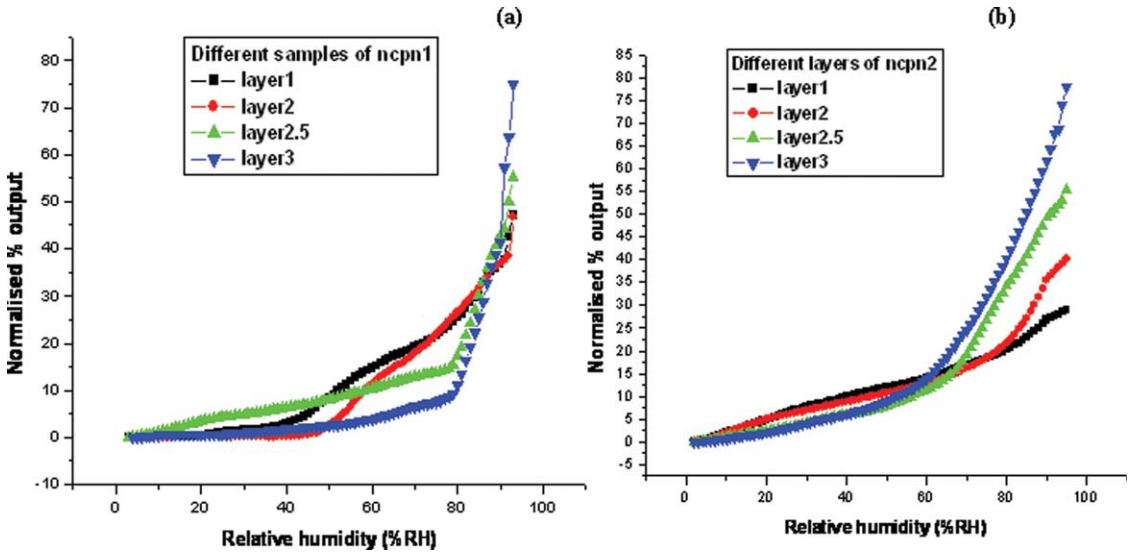

Figure 7 Variation of the percentage output voltage with RH for the number of layers for (a) ncpn1 and (b) ncpn2. [Color figure can be viewed in the online issue, which is available at wileyonlinelibrary.com.]

sample amounts of 5 and 6 μL. For the ncpn2 sample, the sensing mechanism was divided into two regions from all layers.

The increase in the humidity increased the adsorption of water vapors and their condensation in the pores of the film. This led to a scattering of light through the sensing element and, thereby, decreased the output intensity at higher humidity.[22] With increasing thickness for the undoped samples, the bulk mechanism of water increased so its sensitivity decreased in the third region, but with the *m*-NA-doped samples, the adsorption decreased with thickness to cause increases in the sensitivity with thickness in the third region.

TABLE II
Humidity Range and Sensitivity for the Number of Layers for ncpn1 and ncpn2

ncpn1			
Amount of sample (μL)	Sensitivity (mV/% RH)		
	Region I	Region II	Region III
2	0.01292 (3–17)	0.1038 (18–40)	0.64892 (41–93)
4	0.2042 (3–46)	0.8394 (47–66)	0.9906 (67–93)
5	0.45909 (3–79)	3.58601 (80–93)	
6	0.53933 (3–79)	4.60678 (80–93)	

ncpn2		
Amount of sample (μL)	Sensitivity (mV/% RH)	
	Region I	Region II
2	0.86913	2.46804
4	0.60118	2.47876
5	0.72943 (2–76)	5.90293 (77–100)
6	0.88323	6.4247

Sensitivity comparison of the undoped and doped samples with pristine PVA

The comparison of the sensitivity values of the doped and undoped samples with pristine PVA is shown in Figure 8. The third layer was optimized for all of the samples, except ncp1. As shown in Figure 8, PVA acted as a good transmitter of light compared to the undoped and doped samples. When PVA was doped with Co nanoparticles, the rapid transmission decrease meant that the Co nanoparticles might have been good absorbers of water or good scatterers of light. For the *m*-NA-doped samples, the transmittance was between that of PVA and Co/PVA. To understand the effect of Co and *m*-NA on the moisture in detail, the amount of water in the samples was measured gravimetrically at 93 and 0% RH (Fig. 9).

Water content in the undoped and doped samples

With increasing thickness, the water content increased for the undoped samples and decreased for the doped samples. ncp1 had a higher water content than ncp2 at the optimized layer thickness. For undoped samples in the higher RH range, capillary condensation took place to form a meniscus in the samples. With increasing thickness, more water got adsorbed on the sensor and decreased the transmitted intensity of light; hence, the sensitivity started decreasing.[20]

For the doped samples, *m*-NA, being a hydrophobic material, decreased the water intake. At the same time, it provided a lone pair of electrons on the nitrogen from the amine group, which is a functional group of *m*-NA, and enhanced the number of

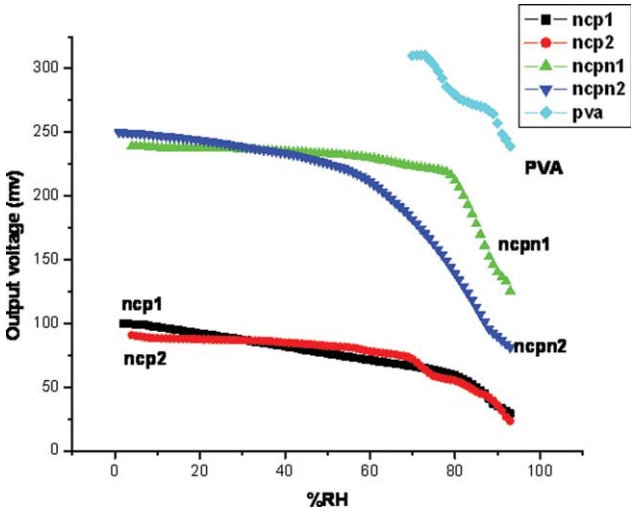

Figure 8 Variation of the output voltage with RH for ncp1, ncp2, ncpn1, ncpn2, and PVA for optimized layers (third layer). [Color figure can be viewed in the online issue, which is available at wileyonlinelibrary.com.]

sites available for the reaction, which enhanced its sensitivity. An effort was made to understand the mechanism to determine the number of sites in the sample, which affected the amount of free water.

Mechanism for the undoped Co/PVA samples

The neat PVA sample showed a response to the RH in a limited range (70–94% RH, Fig. 5). In the Co/PVA nanocomposite, Co, being metallic nanoparticles, enhanced the range and humidity sensitivity and decreased the transmissivity of the composite. This was because when a water molecule adsorbed on the film surface of the polymer, its got uncurled into straight chains that were aligned with respect to each other.[22] Co^{+} ions got loosely attached to OH^{-} ions, and H^{+} was free for conduction; thus, a higher number of sites was offered for more water adsorption on the sensor surface. However, the available sites were not enough for the number of water molecules. An attempt was made to explain the phenomenon with the bulk mechanism. Two schemes are proposed, the first for the Co/PVA matrix and the second for the *m*-NA-doped Co/PVA matrix, as described later. Both of the schemes are divided into two parts, a and b, in which part a explains the complex structure of the matrix and part b deals with the process of occupation of the sites.

PVA reacted with Co salt to form a Co complex, as shown in Scheme 1(a), where activated sites offered by Co weakly bonded with OH— as shown in Scheme 1(b). A water molecule was chemically adsorbed on an activated site to form an adsorption complex, which subsequently transferred to surface hydroxyl groups. When another water molecule came in contact with an OH— group, hydrogen bonding on the two neighboring hydroxyl groups formed. The top condensed water molecule could not move freely because of the restriction from the two hydrogen bonds. Thus, the first physically adsorbed layer was immobile, and no new hydrogen bonds formed in the first physically adsorbed layer and newly coming water molecules. Therefore, no proton conduction took place at this stage, which exhibited low sensitivity at the low humidity.[23,24]

As water continued to condense on the surface of the sensor, an extra layer on top of the first physically adsorbed layer formed; this was less ordered than the first physically adsorbed layer. If more layers condensed, the ordering from the initial surface gradually disappeared, and protons may have had more freedom to move inside the condensed water through the Grotthuss mechanism and were finally almost identical to the bulk liquid water. Because of the condensed layers of water with increasing humidity, the transmitted intensity gradually decreased.[25] This mechanism indicated that sensor based purely on water-phase protonic conduction was not very sensitive to low humidity, at which the water vapor could rarely form continuous mobile layers on the sensor surface.

During the transmission of light through the film, the rate of absorption of light was proportional to the deposition of water molecules on the pore walls; this led to a greater leakage of light through the sensing element.[26] In turn, the output voltage decreased with increasing RH range (Figs. 6 and 7).

Mechanism for the *m*-NA-doped Co/PVA samples

When *m*-NA was doped in the Co/PVA nanocomposites, the humidity response increased gradually.

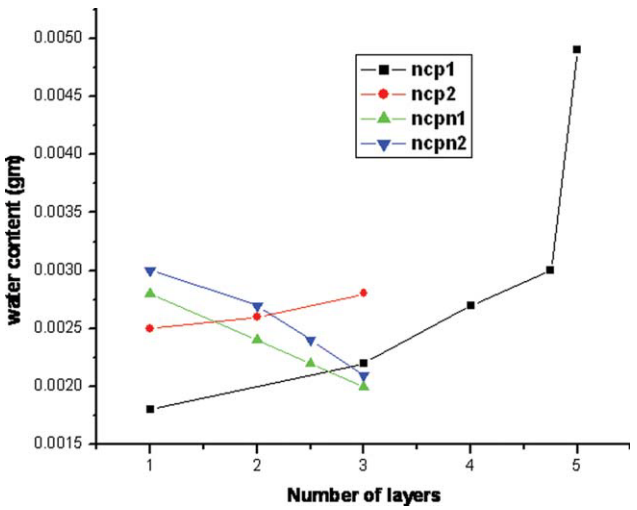

Figure 9 Variation of the water content with the number of layers for the *m*-NA-doped and undoped samples. [Color figure can be viewed in the online issue, which is available at wileyonlinelibrary.com.]

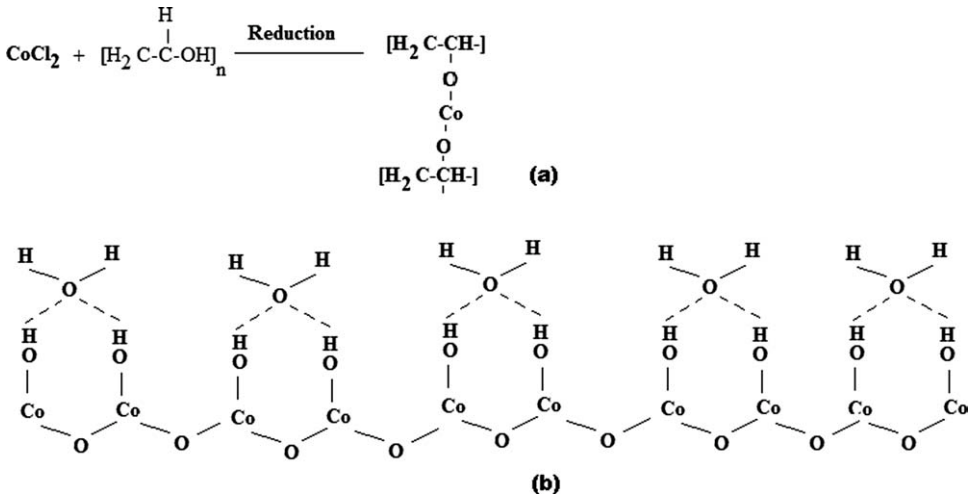

Scheme 1 Simplified physical model of the water adsorption in Co/PVA.

The doping of *m*-NA gave the lone pair of electrons on the nitrogen from the amine, which was a functional group of *m*-NA, which offered some sort of binding with vacant *d* orbitals of Co^0, as shown in Scheme 2(a).[20]

Co^0 ions were loosely attached to the nitrogen by weak Van der Waals' forces of attraction. Hence, greater numbers of protonic sites were available for conduction; this led to a diminished bulk mechanism compared to the undoped samples. The transmittivity was between that of PVA and that of Co/PVA. In support of these two mechanisms and to confirm the effect of moisture, the samples were studied with FTIR spectroscopy.

The FTIR spectra showed the effect of moisture. For convenience, each spectrum is divided into two parts in the spectral regions, that is, 400–1350 cm^{-1} [Fig. 10(a)] and 1351–4000 cm^{-1} [Fig. 10(b)]. From Figure 4, two bands were recognized at 482–490 and 1220 cm^{-1} for ncp1, ncp2, ncpn1, and ncpn2 when they were exposed to a room humidity of about 30–40%. When these samples were exposed to a humidity of about 94%, the band at 482–490 cm^{-1} shifted to 544 cm^{-1}, and there was a broad band formation in the spectral region between 1080 and 1250 cm^{-1}. This broadening of the band was attributed to $O—H^+—O$ stretching and $O—H^+—O$ bending frequencies.[27] Also, broad band formation in the range 600–1000 might have been due to water that arose from liberation, a collective normal mode involving many water molecules.[28]

However, ncp1 did not show any band in the region 1300–1500 [Fig. 10(a)] at room humidity. However, after exposure to humidity (94% RH), a

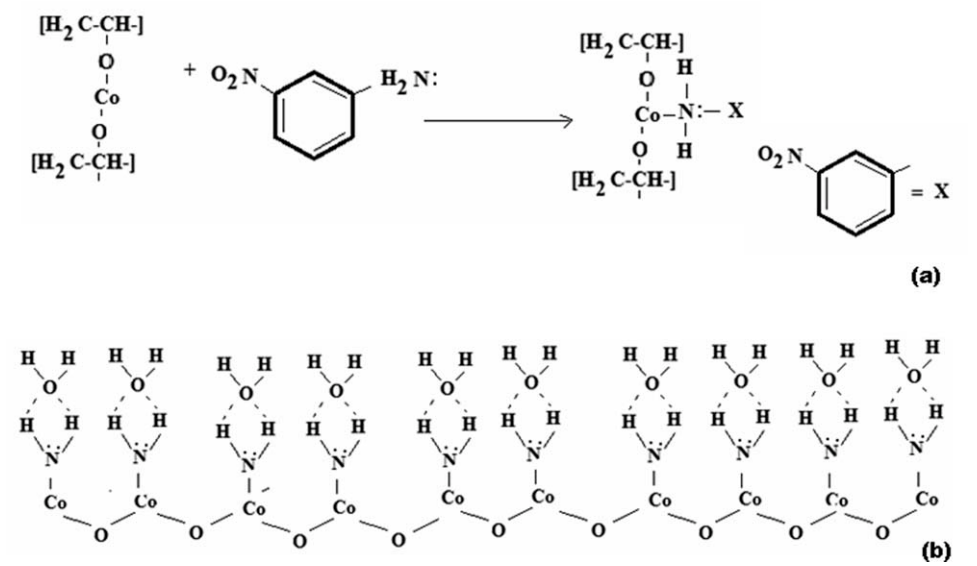

Scheme 2 Simplified physical model of the water adsorption in the *m*-NA-doped Co/PVA.

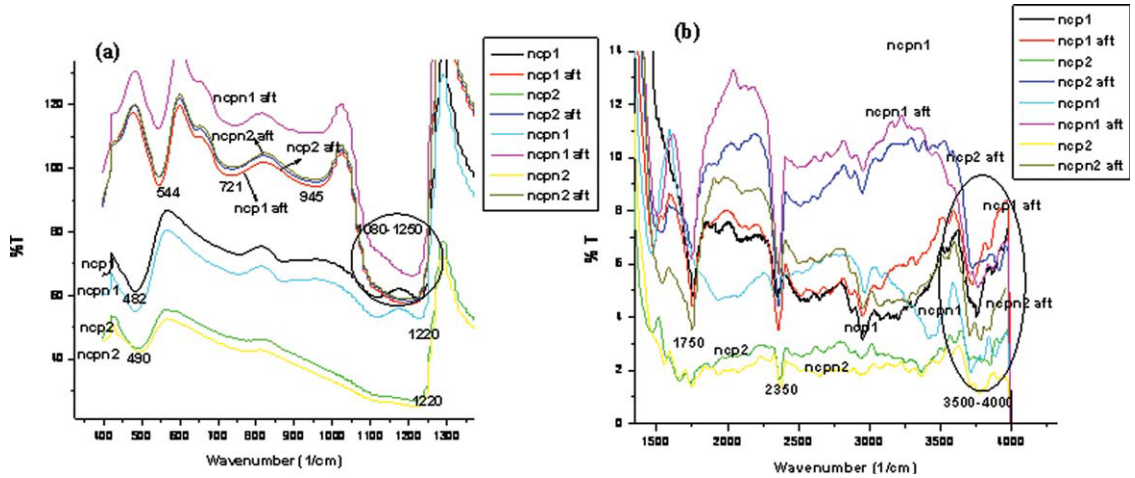

Figure 10 FTIR spectra of ncp1, ncp2, ncpn1, and ncpn2 with and without humidity in the regions (a) 400–1400 and (b) 1450–4000 cm^{-1} (aft, after exposure to humidity). [Color figure can be viewed in the online issue, which is available at wileyonlinelibrary.com.]

new band was introduced at 1490 cm^{-1} due to O—H^+ —O bends.[27] The ncp2 sample had a band at 1450 cm^{-1}, which shifted to 1530 cm^{-1} after it was exposed to humidity. In ncp1 and ncp2, the band at 1750 cm^{-1} became strong with humidity; this was due to H_3O^-.[28] In ncp2, a small band appeared at 1670 cm^{-1} for H_2O bending and disappeared after exposure to humidity and merged into band at 1750 cm^{-1}.

As shown in Figure 10, the band of ncpn1 at 1470 cm^{-1} shifted to 1520 cm^{-1} because of —NH bending. In ncpn1, there was only one band at 2960 cm^{-1}, which became a double band; the broad band in the region 3390–3480 cm^{-1} completely vanished after exposure to humidity. Peaks in the region 2900–4000 cm^{-1} were reduced in ncpn1 and ncpn2 after exposure to humidity, as compared to ncp1 and ncp2. Only ncpn1 and ncpn2 showed peaks at 1500 and 1540 cm^{-1} due to —NH bending when they were exposed to humidity.[29] All of the peaks in the region 2900–4000 cm^{-1} were due to water content.[28]

Recovery and response times

To calculate the response time, all sensors were exposed to 94% RH; here, the response time was the time taken by the sample to reach its saturated output. The response and recovery of both Co samples decreased with increasing weight of Co (56–34 and 176–15 s, respectively), and for the *m*-NA doped samples, the response and recovery times decreased sharply (from 43 to 3 s and from 40 to 10 s, respectively; Fig. 11). It gave a very fast response and recovery compared to Co–polyaniline, that is, 8 s and 1 min, respectively.[30] The amount of water on the doped samples was less than that on the undoped samples, so the rate of absorption (response time)

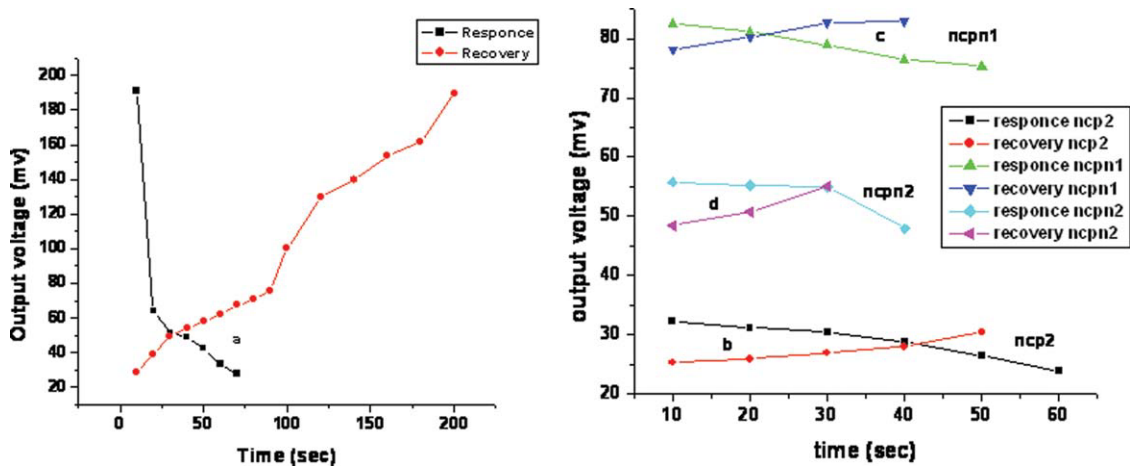

Figure 11 Variation in the response and recovery times for (a) ncp1, (b) ncp2, (c) ncpn1, and (d) ncpn2. [Color figure can be viewed in the online issue, which is available at wileyonlinelibrary.com.]

and desorption (recovery time) was fast in the doped samples.

CONCLUSIONS

A comparative study showed that an *m*-NA-doped humidity sensor was more sensitive than undoped sensors. The doped samples covered the whole range of humidity at the third layer only. The transmittance of the *m*-NA-doped sample was intermediate between PVA and Co/PVA; that is, amount of bulk water was greater in Co/PVA. The water absorption capacity of the *m*-NA-doped sample was lower, but it was more sensitive in the high-humidity region, and its sensitivity increased with the number of layers in the low-humidity region. The doped sensor had a fast response time (3 s) and recovery time (10 s) compared to the undoped sensor.

References

1. Muto, S.; Suzuki, O.; Amano, T.; Morisawa, M. Meas Sci Technol 2003, 14, 746.
2. Melde, B. J.; Johnson, B. J.; Charles, P. T. Sensors 2008, 8, 5202.
3. Rauen, K. L.; Smith, D. A.; Johnso, W. R. H.; Seguin, R.; Stoughton, P. Sens Actuators B 1993, 17, 61.
4. Sakai, Y.; Sadaoka, Y.; Matsuguchi, M.; Sakai, H. Sens Actuators B 1995, 25, 689.
5. Sakai, Y.; Matsuguchi, M.; Hurukawa, T. Sens Actuators B 2000, 66, 135.
6. Tsuchitani, S.; Sugawara, T.; Kinjo, N.; Ohara, S.; Tsunoda, T. Sens Actuators 1988, 15, 375.
7. Sakai, Y.; Matsuguchi, M.; Yonesato, N. Electrochim Acta 2001, 46, 1509.
8. Lee, C. W.; Kim, O. Y.; Gong, M. S. J Appl Polym Sci 2003, 89, 1062.
9. Gong, M. S.; Lee, C. W.; Joo, S. W.; Choi, B. K. J Mater Sci 2002, 37, 4615.
10. Yu, H. H.; Jiang, D. S. Chin J Polym Sci 2002, 20, 1.
11. Sakai, Y.; Sadaoka, Y.; Matsuguchi, M. Sens Actuators B 1996, 35, 85.
12. Ogura, K.; Tonosaki, T.; Shiigi, H. J Electrochem Soc 2001, 148, H21.
13. Nechtschein, M.; Santier, C.; Travers, J. P.; Chroboczek, J.; Alix, A.; Ripert, M. Synth Met 1987, 18, 311.
14. Chiang, J. C.; MacDiarmid, A. G. Synth Met 1986, 13, 193.
15. Angelopoulos, M.; Ray, A.; Mcdiarmid, A. G. Synth Met 1987, 21, 21.
16. Travers, J. P.; Nechtschein, M. Synth Met 1987, 21, 135.
17. Tonosaki, T.; Oho, T.; Isomura, K.; Ogura, K. J Electroanal Chem 2002, 89, 520.
18. Ansari, Z. A.; Karekar, R. N.; Aiyer, R. C. Thin Solid Films 1997, 305, 330.
19. Yang, M. R.; Chen, K. S. Sens Actuators B 1998, 49, 240.
20. Chen, Y.; Liew, K. Y.; Li, J. Appl Surf Sci 2009, 255, 4039.
21. Fuke, M. V.; Vijayan, A.; Kulkani, M.; Hawalder, R.; Aiyer, R. C. Talanta 2008, 76, 1035.
22. Vijayan, A.; Fuke, M. V.; Hawalder, R.; Kulkani, M.; Amalnerkar, D.; Aiyer, R. C. Sens Actuators B 2008, 129, 106.
23. Yadav, B. C.; Shukla, R. K.; Bali, L. M. Ind J Pure Appl Phys 2005, 43, 51.
24. Yadav, B. C.; Pandey, N. K.; Srivastava, A. K.; Sharma, P. Meas Sci Technol 2007, 18, 260.
25. Moromoto, T.; Nagao, M.; Tokuda, F. J Phys Chem 1969, 73, 243.
26. Yadav, B. C.; Yadav, R. C.; Dube, G. C. Opt Appl 2009, 3, 1.
27. Sauer, J.; Dçbler, J. Chem Phys Chem 2005, 6, 1706.
28. Laporta, M.; Pegoraro, M.; Zanderighi, L. Phys Chem Chem Phys 1999, 1, 4619.
29. Pal, K.; Banthia, A. K.; Majumdar, D. K. AAPS Pharm Sci Tech 2007, 8, 21.
30. Fuke, M. V.; Adhyapak, P. V.; Mulik, U. P.; Amalnerkar, D. P.; Aiyer, R. C. Talanta 2009, 78, 590.